Mathematical Biosciences and Engineering

MBE, 20(12): 20468–20485.
DOI: 10.3934/mbe.2023905
Received: 22 July 2023
Revised: 10 October 2023
Accepted: 30 October 2023
Published: 13 November 2023

http://www.aimspress.com/journal/MBE

Research article

Suppression of absence seizures by using different stimulations in a reduced corticothalamic-basal ganglion-pedunculopontine nucleus model

Xiaolong Tan, Rui Zhu, Yan Xie and Yuan Chai*

School of Mathematics and Physics, Shanghai University of Electric Power, Shanghai 201306, China

* **Correspondence:** Email: chaiyuan@shiep.edu.cn.

Abstract: Coupled neural network models are playing an increasingly important part in the modulation of absence seizures today. However, it is currently unclear how basal ganglia, corticothalamic network and pedunculopontine nucleus can coordinate with each other to develop a whole coupling circuit, theoretically. In addition, it is still difficult to select effective parameters of electrical stimulation on the regulation of absence seizures in clinical trials. Therefore, to develop a coupled model and reduce computation cost, a new model constructed by a simplified basal ganglion, two corticothalamic circuits and a pedunculopontine nucleus was proposed. Further, to seek better inhibition therapy, three electrical stimulations, high frequency stimulation (HFS), 1:0 coordinate reset stimulation (CRS) and 3:2 CRS, were applied to the thalamic reticular nucleus (RE) in the first corticothalamic circuit in the coupled model. The simulation results revealed that increasing the frequency and pulse width of an electrical stimulation within a certain range can also suppress seizures. Under the same parameters of electrical stimulation, the inhibitory effect of HFS on seizures was better than that of 1:0 CRS and 3:2 CRS. The research established a reduced corticothalamic-basal ganglion-pedunculopontine nucleus model, which lays a theoretical foundation for future optimal parameters selection of electrical stimulation. We hope that the findings will provide new insights into the role of theoretical models in absence seizures.

Keywords: absence seizure; corticothalamic circuit; electrical stimulation; coordinate reset stimulation; high frequency stimulation

1. Introduction

Absence epilepsy is a common neurological disease of the brain that usually occurs in

childhood [1–3]. It is characterized by a spike wave discharge (SWD) occurring in the electroencephalogram (EEG) with a frequency of 2–4 Hz [4–6]. Absence epilepsy can lead to cognitive and learning disabilities and temporary loss of consciousness, and these symptoms are related to the abnormality of corticothalamic circuits [7,8]. Recent studies have shown that the reticular nucleus of the thalamus acts as a pacemaker in the control of an absence seizure [9–11]. Similarly, much research evidence shows that the basal ganglia is also involved in the control of absence seizure by the corticothalamic circuit [12–14]. To more conveniently study how the basal ganglia is involved in controlling absence seizure, Fan et al. [15] simplified the basal ganglia into a theoretical model of 3I:2O modulator to study the regulation of basal ganglia on absence seizure. In addition, some scholars have used the mean field model to analyze the dynamic state of neurons in absence epilepsy. Robinson et al. [16] established a corticothalamic network through the mean field model and successfully simulated the EEG under normal and seizure states. Chen et al. [17] established a basal ganglia-corticothalamic (BGCT) model through the mean model to describe the physiological mechanism of neuronal firing. Jiruska et al. [18] made an in-depth study on the theoretical mechanism of synchronization and desynchronization of epileptic seizures. However, most of the research only focuses on the network composed of a single corticothalamic circuit and basal ganglia or two corticothalamic circuits without considering the influence of the basal ganglia. Therefore, it is necessary to further establish a model composed of two corticothalamic circuits and basal ganglia.

The first motivation of the research was to investigate an expanding model to extend the original single-compartment cortico-thalamic model by coupling other neurons. In addition to the basal ganglia and corticothalamus related to absence seizures, there are also some studies indicating that the pedunculopontine nucleus (PPN) is also involved in the regulation of some neurological diseases [19], and some scholars have established a theoretical model consisting of the corticothalamic circuit, basal ganglia and PPN [20–22]. Inspired by these models, we introduced a PPN structure into the model to explore the physiological mechanism of seizures. In the human brain, PPN controls movement through gamma amino butyric acid energy (GABAergric) and glutamatergic neurons [23,24]. Some experimental studies have shown that PPN is also closely related to basal ganglia. PPN projects signals to the subthalamic nucleus (STN) and globus pallidus internal (GPi) of basal ganglia, and STN also gives feedback signals to the PPN [24,25]. Niktarash et al. [26] established a coupling theoretical network between the two based on the projection effect of PPN on GPi. In addition to being connected to the basal ganglia, the experimental study by Wang et al. [27] shows that PPN can project choline to the thalamic reticular nucleus. These findings provide theoretical guidance for us to further improve the pathogenesis of absence seizure.

The second motivation of the research was to identify an optimal suppressive scheme by contrasting different stimulus paradigms and many stimulus parameters. Although there are many clinical trials on neurological diseases, it is difficult to achieve good results through drug treatment for some patients with seizures [28]. For a small number of patients with seizures, it can take surgical resection to achieve good treatment results [29]. However, some patients with seizures are still difficult to treat. As a new method of treating neurological diseases, electrical stimulation is widely used in clinical treatment and theoretical model research [30–32]. Wang et al. [9] established a theoretical model to study the effect of electrical stimulation on absence seizures and concluded that electrical stimulation can suppress seizures well. In addition, some scholars have also studied the effect of electrical stimulation on seizures through animal experiments and made in-depth research on the mechanism of electrical stimulation [33–35]. Recently, coordinated reset stimulation (CRS) was used

to study the suppression of seizures as a pulse sequence sent to a specific part of the brain within a specific period of time [36–38]. Fan et al. [15] used high frequency CRS to stimulate the various structures of the basal ganglia and achieved a good inhibitory effect on seizures. In addition, high frequency pulses are also used in animal experiments to study the relationship between the thalamic reticular nucleus and seizures [39].

However, previous models only considered interactions between a single corticothalamic network and the basal ganglia or two corticothalamic networks. For example, although the 3I:2O model simplifies the basal ganglia, which improves the running time of computing, it cannot reveal more complex neural connection pathways. Therefore, we established a model consisting of two cortical thalamic circuits, PPN and simplified basal ganglia based on the 3I:2O model, which can study more complex neural connection pathways. It is also possible to study the effect of electrical signals passing through the PPN on the electrical signals of the cerebral cortex. Although the model has become more complex, the calculation runs in less time than the non-simplified model. In terms of the effect of electrical stimulation on the brain, previous studies have only explored the inhibitory effect of fixed parameters on seizure. Therefore, solving inhibitory control problems needs much more exploration.

The key contribution of this research has three main creations. First, we simplified the basal ganglia into a modulator, which can efficiently receive signals from other parts. Second, we found that increasing the coupling strength of some pathways can suppress absence seizures. Third, we applied three different forms of electrical stimulation to the thalamic reticular nucleus and explored how the electrical stimulation parameters inhibited SWD under changing conditions.

2. Model and mathematical methods

To analyze the dynamic state of the basal ganglia, corticothalamic circuit and PPN, we built a reduced BGCT-PPN model, as shown in Figure 1. The model was composed of six types of neurons: Excitatory pyramidal neurons (PY_1 and PY_2); inhibitory interneurons (IN_1 and IN_2); thalamic relay nuclei (TC_1 and TC_2); thalamic reticular nucleus (RE_1 and RE_2); simplified basal ganglia modulator (3I:5O); PPN. The basal ganglia were simplified to a 2I:3O modulator in the previous study [9]. In the model of this paper, it's simplified to a modulator with three inputs and five outputs stimulation. The mean field model is described [40–42]:

$$M_y(r,t) = S\left[V_y(r,t)\right] = \frac{M_y^{max}}{1+exp\left[-\frac{\pi\left(V_y(r,t)-\theta_y\right)}{\sqrt{3}\sigma_y}\right]}, \tag{1}$$

where $y \in \{p_1, p_2, i_1, i_2, t_1, t_2, r_1, r_2, m, ppn\}$ represents the combination of different types of neuron populations, p_1 and p_2 represent two different excitatory pyramidal neurons in the model, i_1 and i_2 represent inhibitory interneurons in two different parts, t_1 and t_2 represent two different thalamic relay nuclei in the model, r_1 and r_2 represent two different thalamic reticular nuclei in the model, m represents the simplified basal ganglia and *ppn* is the pedunculopontine nucleus. M_y^{max} is the maximum mean discharge rate of neuron population and y. θ_y is the firing threshold of each neuron population. σ_y is the standard deviation of the mean discharge threshold. The potential change in the cell can be expressed as follows [43–45]:

$$D_{\alpha\beta}V_y(t) = \sum_x \upsilon_{yx}\,\varphi_x\left(t-\tau_{yx}\right), \tag{2}$$

$$D_{\alpha\beta} = \frac{1}{\alpha\beta}\left[\frac{\partial}{\partial t^2} + (\alpha+\beta)\frac{\partial}{\partial t} + \alpha\beta\right], \tag{3}$$

v_{yx} representing the coupling strength of neuron population x to y. φ_x is the input transmission rate. τ_{yx} is the axon time delay from neuron x to y. $D_{\alpha\beta}$ represents the axonal and dendritic filtering of the input signal. α and β are the attenuation and rise time of the input signal.

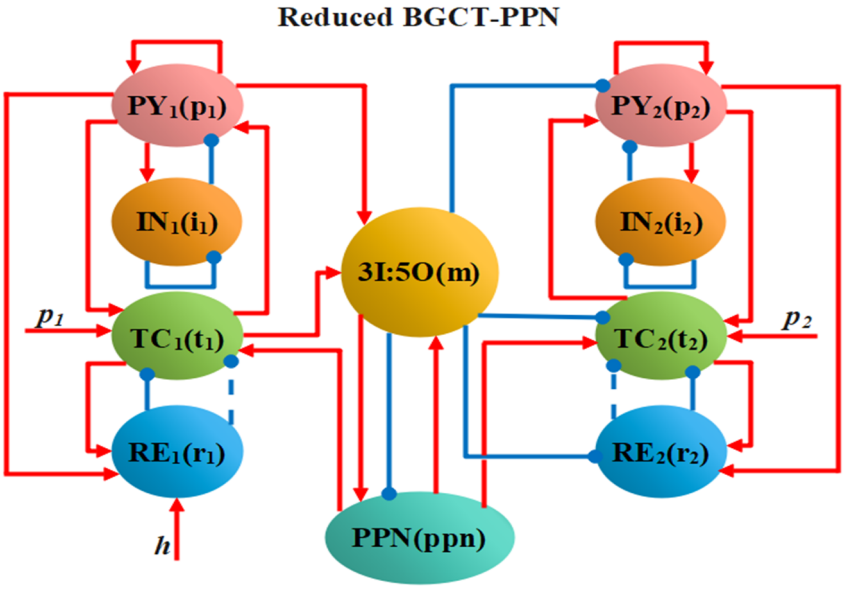

Figure 1. Reduced BGCT-PPN model. The model consists of four parts, i.e., the first corticothalamic circuit (PY_1, IN_1, TC_1 and RE_1), the second corticothalamic circuit (PY_2, IN_2, TC_2 and RE_2), 3I:5O modulator and PPN. Red arrow indicates the excitatory stimulation mediated by glutamate as the receptor. Blue solid line and dashed line indicate inhibitory stimulation mediated by $GABA_A$ and $GABA_B$ as receptors, respectively.

Robinson et al. proposed a damped wave equation propagating in the axon field as shown below [46–48]:

$$\frac{1}{\gamma_y^2}\left[\frac{\partial^2}{\partial t^2}+2\gamma_y\frac{\partial}{\partial t}+\gamma_y^2\right]\varphi_y(t)=M_y(t), \tag{4}$$

where $\gamma_y = v_y/r_y$ represents the damping rate of propagation, r_y represents the characteristic range of axons and v_y is the rate of signal conduction in the axon. In the paper, we only considered the damping rate of cortical excitatory pyramidal neurons. To facilitate the calculation, we set $M_p = M_i$ and $V_p = V_i$, where p and i represent excitatory pyramidal neurons and inhibitory interneurons, respectively.

Based on previous research, we combined the basal ganglia, corticothalamic circuit and PPN as a new model, and the mathematical equations were described as follows:

The kinetic equations of PY_1 under its own and external stimuli are as follows:

$$\frac{d\dot{\phi}_{p_1}}{dt}=\gamma_p^2\{-\phi_{p_1}(t)+S[V_{p_1}(t)]\}-2\gamma_p\dot{\phi}_{p_1}, \tag{5}$$

$$\frac{d\dot{V}_{p_1}}{dt}=\alpha\beta\{-V_{p_1}(t)+v_{p_1p_1}\phi_{p_1}(t)-v_{p_1i_1}S[V_{i_1}(t)]+v_{p_1t_1}S[V_{t_1}(t)]\}-(\alpha+\beta)\dot{V}_{p_1}(t). \tag{6}$$

The kinetic equation of TC_1 stimulated by the surrounding nervous nuclei is shown below:

$$\frac{d\dot{V_{t_1}}}{dt} = \alpha\beta\begin{Bmatrix}-V_{t_1}(t) + v_{t_1p_1}\phi_{p_1}(t) - v_{t_1r_1}^{A}S\left[V_{r_1}(t)\right] - v_{t_1r_1}^{B}S\left[V_{r_1}(t-\tau)\right]\\ +P_1 + v_{t1ppn}S[V_{ppn}(t)]\end{Bmatrix} - (\alpha+\beta)\dot{V_{t_1}}(t). \quad (7)$$

From Figure 1 and the above equation, the following dynamic equation of state of the thalamic reticular nucleus can be obtained:

$$\frac{d\dot{V_{r_1}}}{dt} = \alpha\beta\left\{-V_{r_1}(t) + v_{r_1p_1}\phi_{p_1}(t) + v_{r_1t_1}S\left[V_{t_1}(t)\right] + h_{DBS}(t)\right\} - (\alpha+\beta)\dot{V_{r_1}}(t). \quad (8)$$

In the same way, we can obtain the dynamic equation of the discharge of the nucleus of the second corticothalamic circuit in Figure 1:

$$\frac{d\dot{\phi}_{p_2}}{dt} = \gamma_p^2\left\{-\phi_{p_2}(t) + S\left[V_{p_2}(t)\right]\right\} - 2\gamma_p\dot{\phi}_{p_2}, \quad (9)$$

$$\frac{d\dot{V_{p_2}}}{dt} = \alpha\beta\begin{Bmatrix}-V_{p_2}(t) + v_{p_2p_2}\phi_{p_2}(t) - v_{p_2i_2}S\left[V_{i_2}(t)\right]\\ +v_{p_2t_2}S\left[V_{t_2}(t)\right] - O_1\end{Bmatrix} - (\alpha+\beta)\dot{V_{p_2}}(t), \quad (10)$$

$$\frac{d\dot{V_{t_2}}}{dt} = \alpha\beta\begin{Bmatrix}-V_{t_2}(t) + v_{t_2p_2}\phi_{p_2}(t) - v_{t_2r_2}^{A}S\left[V_{r_2}(t)\right] + P_2\\ -v_{t_2r_2}^{B}S\left[V_{r_2}(t-\tau)\right] + v_{t_2ppn}S\left[V_{ppn}(t)\right] - O_2\end{Bmatrix} - (\alpha+\beta)\dot{V_{t_2}}(t), \quad (11)$$

$$\frac{d\dot{V_{r_2}}}{dt} = \alpha\beta\begin{Bmatrix}-V_{r_2}(t) + v_{r_2p_2}\phi_{p_2}(t)\\ +v_{r_2t_2}S\left[V_{t_2}(t)\right] - O_3\end{Bmatrix} - (\alpha+\beta)\dot{V_{r_2}}(t), \quad (12)$$

$$\frac{d\dot{V}_{ppn}}{dt} = \alpha\beta\left\{-V_{ppn}(t) + O_4 - O_5\right\} - (\alpha+\beta)\dot{V}_{ppn}(t). \quad (13)$$

Most of the parameters of the formula are from the papers [17,22]. A small part of the parameter was changed within a normal physiological range. The detailed results of the parameters were shown in Tables 1 and 2.

Table 1. Default parameters.

Parameters	Meaning	Value
$M_{p_1,p_2}^{max_{i_1,i_2}^{max}}$	Cortical maximum firing rate	250 Hz
M_{t_1,t_2}^{max}	SRN maximum firing rate	250 Hz
M_{r_1,r_2}^{max}	TRN maximum firing rate	250 Hz
M_{ppn}^{max}	Connector maximum firing rate	200 Hz
θ_{i_1,i_2}	Mean firing rate threshold of cortical	15 mV
θ_{t_1,t_2}	Mean firing rate threshold of SRN	15 mV
θ_{r_1,r_2}	Mean firing rate threshold of TRN	15 mV
θ_{ppn}	Mean firing rate threshold of Connector	9 mV
γ_p	Cortical damping rate	100 Hz
τ	Delay time	80 ms
α	Synaptodendritic decay time constant	50 s^{-1}
β	Synaptodendritic rise time constant	200 s^{-1}
σ	Threshold variability of firing rate	6 mV
$P_{1,2}$	Nonspecific input	10 mV s

Table 2. Strength of coupling.

Parameters	Source	Target	Value
$v_{p_1p_1}$	PY_1	PY_1	1 mV s
$v_{p_1i_1}$	IN_1	PY_1	1.8 mV s
$v_{r_1p_1}$	PY_1	RE_1	0.05 mV s
$v_{r_1t_1}$	TC_1	RE_1	0.5 mV s
$v_{t_1p_1}$	PY_1	TC_1	2.2 mV s
$v_{t_1r_1}^{A,B}$	RE_1	TC_1	0.8 mV s
$v_{p_1t_1}$	TC_1	PY_1	1.8 mV s
$v_{p_2p_2}$	PY_2	PY_2	1 mV s
$v_{p_2i_2}$	IN_2	PY_2	1.8 mV s
$v_{r_2p_2}$	PY_2	RE_2	0.05 mV s
$v_{r_2t_2}$	TC_2	RE_2	0.5 mV s
$v_{t_2p_2}$	PY_2	TC_2	2.2 mV s
$v_{t_2r_2}^{A,B}$	RE_2	TC_2	0.8 mV s
$v_{p_2t_2}$	TC_2	PY_2	1.8 mV s
v_{t_1ppn}	PPN	TC_1	0.03 mV s
v_{t_2ppn}	PPN	TC_2	0.03 mV s
O_1	m	PY_2	8 mV s
O_2	m	TC_2	1.75 mV s
O_3	m	RE_2	1.75 mV s
O_4	m	PPN	2.2 mV s
O_5	m	PPN	0.15 mV s

To further study the control mechanism of seizures, we applied electrical stimulation to the model TC_1. The forms of electrical stimulation are HFS, 1:0 CRS and 3:2 CRS. Their pulse diagram was shown in Figure 2. The mathematical expression of HFS was described as follows [9,49,50]:

$$h_{DBS}(t) = A * H\left(sin(\frac{2\pi}{T}t)\right)\left(1 - H\left(sin(\frac{2\pi(t+p_0)}{T})\right)\right), \tag{14}$$

$$a(t) = -(A * \frac{|sin(2\pi*(t/(8*T)))|}{sin(2\pi*(t/(8*T)))} + A)/2, \tag{15}$$

$$b(t) = -(A * \frac{|sin(2\pi*(t/(40*T)))|}{sin(2\pi*(t/(40*T)))} - A)/2, \tag{16}$$

$$r(t) = h_{DBS}(t) - a(t) - A. \tag{17}$$

If $r < 0$, we set $r = 0$, and the formula for 1:0 CRS is

$$h_{1:0\ CRS} = r, \tag{18}$$

$$L = r - b(t), \tag{19}$$

when $L < 0$, we set $L = 0$, and 3:2 CRS can be described as

$$h_{3:2\ CRS} = L. \tag{20}$$

In the HFS formula, A represents the amplitude of the electrical stimulation and T and p_0 represent the period and width of the pulse oscillation, respectively. The t and H in the electrical stimulation equation represent the time and heaviside function, respectively. In this paper, we gave stimulation time to the reticular nucleus of thalamus 10 s in the model, according to the electrical stimulation form of Figure 2. In the process of modeling electrical stimulation, we constructed two different square wave functions based on HFS pulse sequence, and then we obtained two forms of CRS by superimposing the two square wave functions with HFS, respectively. Both HFS and CRS are single-phase pulse stimulations, of which CRS is divided into 1:0 CRS and 3:2 CRS in Figure 2 due to the different distribution of pulse sequences.

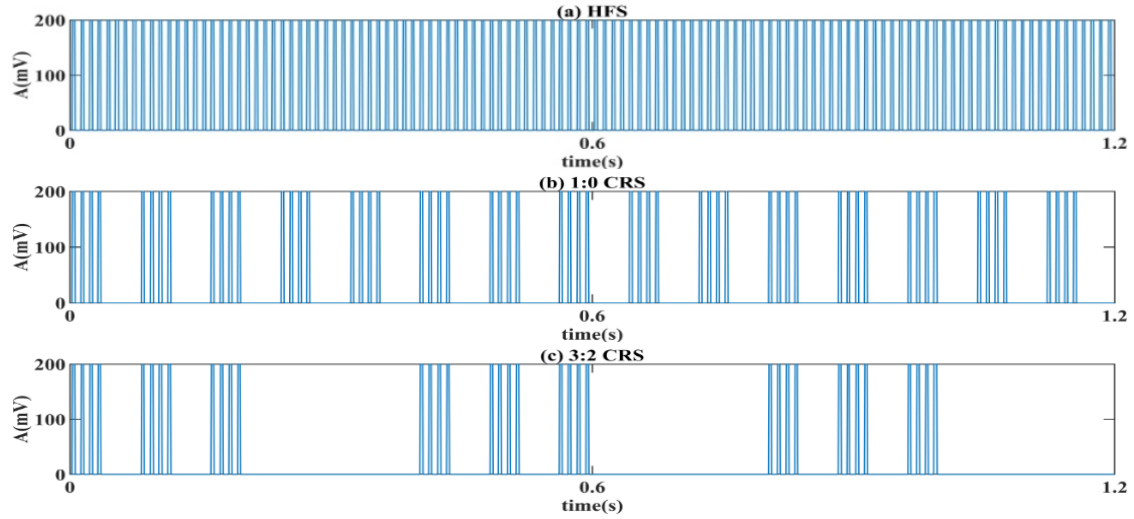

Figure 2. Different forms of electrical stimulation. (a) HFS. (b) 1:0 CRS. (c) 3:2 CRS. The pulse width of electrical stimulation can be set as 1–3 ms, the frequency of electrical stimulation can be set between 100–185 Hz and the intensity of electrical stimulation is 0–200 mV.

3. Results

3.1. Dynamic state and frequency analysis of neuron firing

The thalamus plays an important role in controlling seizures through $GABA_B$ synapses, especially in the pathway between TC and RE [51–53]. To verify this effect of the thalamus, the state and frequency of epileptic area was analyzed in Figure 3 by a 2D (v_{t1r1}, τ) panel. It can be seen from Figure 3(a),(b) that when v_{t1r1} was small, only saturation state appeared. When time increased, the discharge frequency of the cerebral cortex increased to the maximum and the saturation state was shown in Figure 3(c). If v_{t1r1} continued to increase, SWD appeared, indicating a seizure. It can be seen from Figure 3(b) that the oscillation frequency of the SWD was 2–4 Hz. In addition, the frequencies of simple oscillations were also partially located at 2–4 Hz, but the difference from SWD was shown in Figures 3(d),(e). Simple oscillation had only one peak in one cycle and SWD had two peaks. When v_{t1r1} increased to the maximum, there was a low firing state. As shown in Figure 3(f), the firing became a straight line with an oscillation frequency of zero Hz as time increased. From the above analysis and results in Figure 3, it can be known that the model in this paper can successfully simulate four dynamic states of the cerebral cortex.

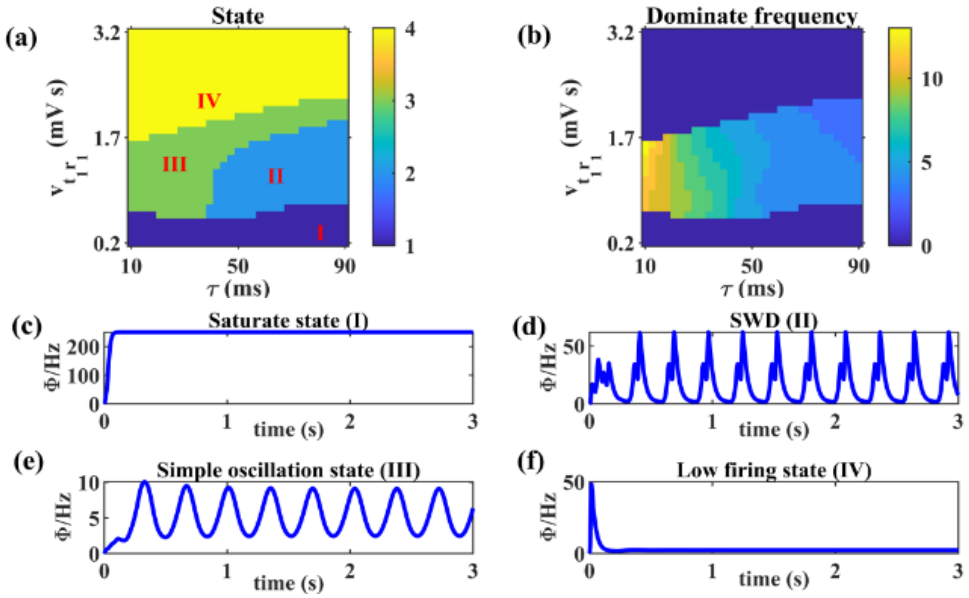

Figure 3. Dynamic states of neuron firing. (a) Four dynamic states. (b) The frequency distribution of four dynamic states. (c) Saturate state, $v_{t1r1} = 0.2$ mV, $\tau = 80$ ms. (d) SWD, $v_{t1r1} = 1$ mV s, $\tau = 80$ ms. (e) Simple oscillation state, $v_{t1r1} = 2.1$ mV s, $\tau = 80$ ms. (f) Low firing state, $v_{t1r1} = 3.2$ mV s, $\tau = 80$ ms.

3.2. Effect of electrical stimulation parameters and the coupling strength of TC$_1$ to RE$_1$ pathway on neuronal dynamics

The electrical stimulation parameters and the coupling strength $v_{t_1r_1}$ were used to explore the suppression of seizures. Figure 4(a),(b) shows the effect of HFS on neuronal dynamics and dominant frequency, respectively. Figure 4(c),(d) shows the effect of stimulation on neuronal dynamics and dominant frequency after applying 1:0 CRS on RE$_1$. The effect of 3:2 CRS on the dynamics and dominant frequency of neurons is shown in Figure 4(e),(f). Figure 4 shows that the SWD areas of HFS, 1:0 CRS and 3:2 CRS account for 3.58, 7.48 and 17.46%, respectively. As the coupling strength and electrical stimulation intensity increased, the SWD area gradually became smaller. It was concluded that the inhibitory effect of HFS on seizures is better than CRS, and the therapeutic effect of 1:0 CRS is better than 3:2 CRS. Therefore, for a better therapeutic effect, we could increase the electrical stimulation intensity and coupling strength in a certain range.

Figure 5 explores the effect of electrical stimulation on the dynamics state of neurons in the (v_{t1r1}, p_0) panel. Figure 5(a),(b) shows the dynamic states and frequency analysis after adding HFS. It can be seen from the figure that when the pulse width increased appropriately, the area of SWD area gradually decreases and accounts for 3.36% of the whole dynamic state. Figure 5(c),(d) shows that after applying 1:0 CRS to RE$_1$, we found that its change trend is like that of HFS. In the process of increasing the pulse width, the area of SWD also decreases gradually. The SWD area with 1:0 CRS was obviously larger than the SWD area with HFS. Figure 5(e),(f) shows the effect of 3:2 CRS on RE$_1$. Compared with the above two methods, 3:2 CRS has a relatively weak inhibition effect on SWD, and the SWD area accounts for 42.86%.

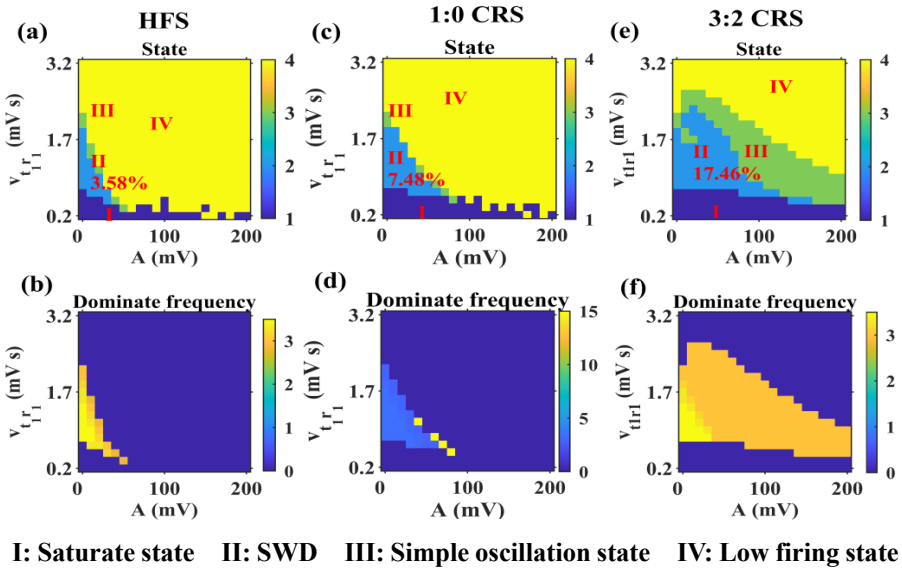

Figure 4. Influence of electrical stimulation on neuron dynamics in (v_{t1r1}, A) panel. (a) and (b) represent the influence of HFS on the dynamic state and oscillation frequency of neurons. (c) and (d) represent the influence of 1:0 CRS on the dynamic state and oscillation frequency of neurons. (e) and (f) represent the influence of 3:2 CRS on the dynamic state and oscillation frequency of neurons. During the whole electrical stimulation, we set $p_0 = 1$ ms, $T = 120^{-1}$ s and $\tau = 80$ ms.

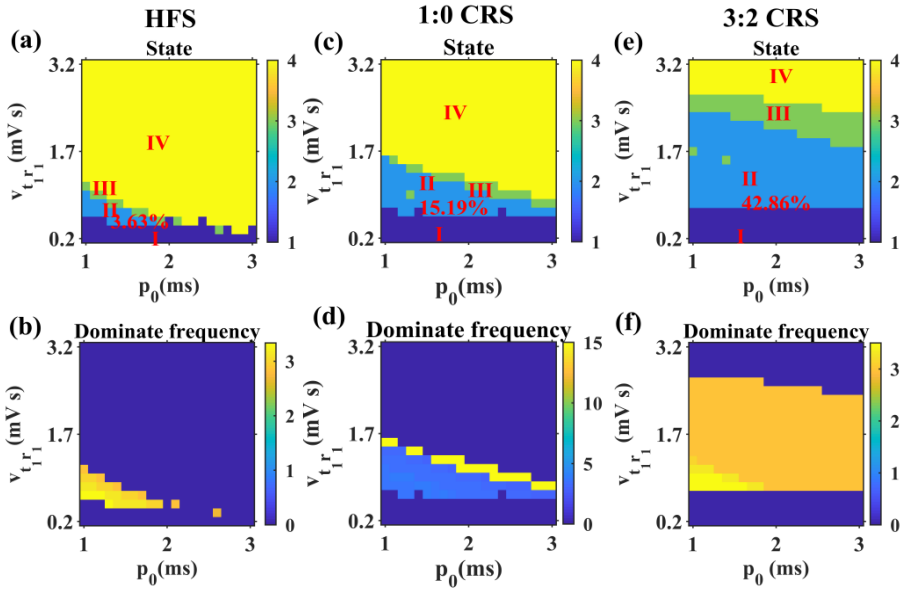

Figure 5. Influence of electrical stimulation on neuron dynamics in the (v_{t1r1}, p_0) panel. (a) and (b) represent the influence of HFS on the dynamic state and oscillation frequency of neurons. (c) and (d) represent the influence of 1:0 CRS on the dynamic state and oscillation frequency of neurons. (e) and (f) represent the influence of 3:2 CRS on the dynamic state and oscillation frequency of neurons. When electrical stimulation was applied, the period and intensity of stimulation were $T = 120^{-1}$ s and $\mathrm{A} = 120$ mV.

Figure 6 explores the effect of coupling strength and electrical pulse stimulation frequency on the SWD area. Figure 6(a),(b) shows the suppression effect after adding HFS. When the frequency of electrical stimulation increases, the SWD area is greatly reduced, accounting for only 0.45% of the whole state. The influence of 1:0 CRS on the dynamic state and main frequency of neurons was shown in Figure 6(c),(d). When the stimulation frequency increased, the area of SWD began to decrease significantly, and finally accounted for 12.02% of the whole state area. The impact of 3:2 CRS on neuronal activity was shown in Figure 6(e),(f). Its trend of change was the same as that of HFS and 1:0 CRS, but its SWD area was larger, accounting for 34.01%.

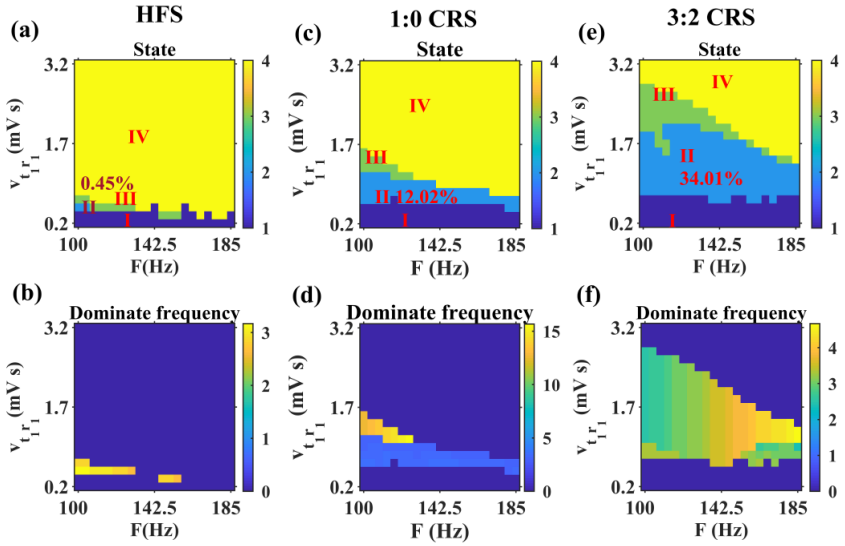

Figure 6. Influence of electric electrical stimulation on neuron dynamics in the (v_{t1r1}, F) panel. (a) and (b) represent the influence of HFS on the dynamic state and oscillation frequency of neurons. (c) and (d) represent the influence of 1:0 CRS on the dynamic state and oscillation frequency of neurons. (e) and (f) represent the influence of 3:2 CRS on the dynamic state and oscillation frequency of neurons. The intensity and pulse width of electrical stimulation are set to $A = 120$ mV and $p_0 = 1$ ms, respectively.

3.3. Influence of electrical stimulation parameters on neuron dynamics

Figure 7 shows the inhibitive effect of applying various electrical stimulation to RE_1 in the (F, A) panel. Figure 7(a),(b) shows the inhibitive effect of HFS on neuronal activity. When the electrical stimulation intensity continues to increase, the SWD area will gradually decrease and then disappear, and the increase of electrical stimulation frequency will also lead to the decrease of the SWD area and, finally, the percentage of the SWD area is 12.70%. Figure 7(c) shows the relationship between the electrical stimulation intensity and frequency of HFS and the number of SWD. From the figure, we can know that the increase of electrical stimulation intensity and frequency will greatly reduce the number of SWD. Figure 7(d),(e) shows the impact of 1:0 CRS on the state and frequency of neuron firing activity. Its influence on SWD area change is like the dynamic state under the influence of HFS, but the percentage of the SWD area is 25.85%. Figure 7(f) is about the relationship between stimulation intensity and the frequency of 1:0 CRS and SWD quantity. With the increase of electrical stimulation intensity and frequency, the SWD quantity begins to decrease gradually, but the decreasing trend of

SWD quantity is not as fast as that under the influence of HFS. Figure 7(g),(h) respectively shows the effect of 3:2 CRS on neuron discharge activity. Its SWD area percentage is 45.58%, which is far weaker than the inhibition effect of the above two kinds of electrical stimulation on SWD. Figure 7(i) is the relationship between the parameter changes of 3:2 CRS and the number of SWD. We can find that the number of SWD will decrease slowly with the increase of electrical stimulation intensity and frequency.

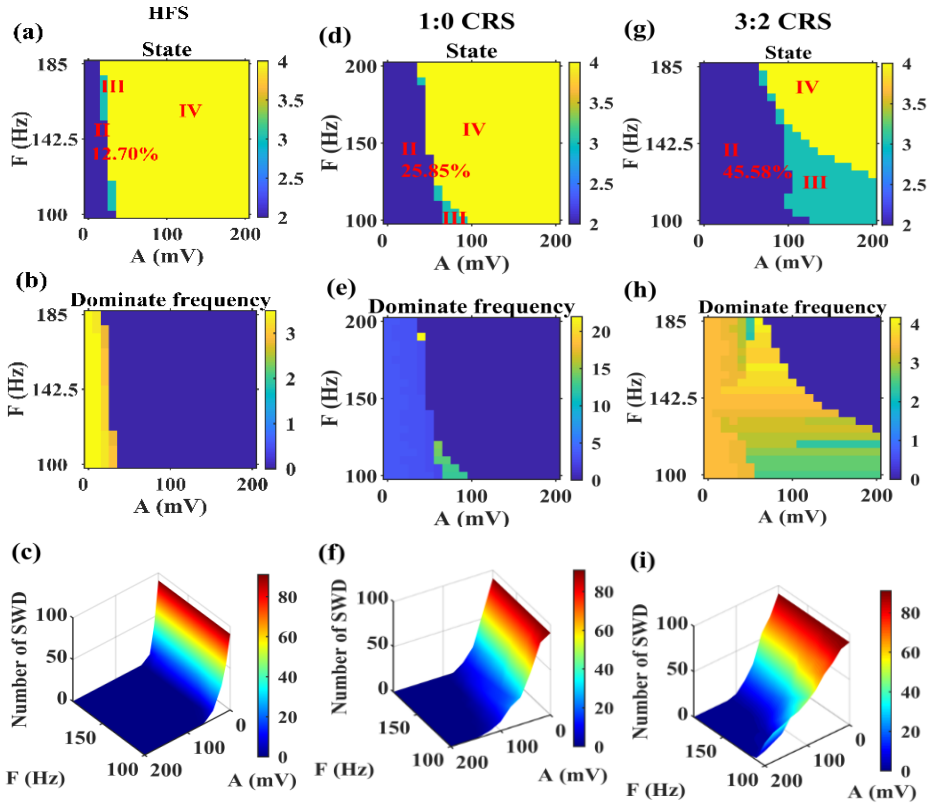

Figure 7. Influence of electrical stimulation on neuron dynamics in the (F, A) panel. (a) and (b) represent the influence of HFS on the dynamic state and oscillation frequency of neurons. (c) is the relationship between the stimulation intensity and frequency of HFS and the number of SWD. (d) and (e) represent the influence of 1:0 CRS on the dynamic state and oscillation frequency of neurons. (f) is the relationship between the stimulation intensity and frequency of 1:0 CRS and the number of SWD. (g) and (h) represent the influence of 3:2 CRS on the dynamic state and oscillation frequency of neurons. (i) is the relationship between the stimulation intensity and frequency of 3:2 CRS and the number of SWD. The pulse width of the electrical stimulation is $p_0 = 1$ ms.

Figure 8 represents the effect of electrical stimulation on the dynamic states and firing frequency of neurons in the (p_0, A) panel. Figure 8(a),(b) shows the effect of HFS on the discharge activities of neurons. With the increase of electrical stimulation intensity and pulse width, the SWD area will decrease greatly, accounting for 9.07% of the whole state area. Figure 8(c) shows the influence of the intensity and frequency of HFS on the number of SWD. With the increase of these two parameters, the number of SWD will decrease greatly, which shows that increasing the intensity and pulse width of electrical

stimulation has an obvious effect on inhibiting SWD. The impact of 1:0 CRS on the neuron firing state and frequency was shown in Figure 8(d),(e). The SWD area change was also like the change trend of the SWD area under the HFS. However, the SWD area of 1:0 CRS, a larger one, accounted for 17.01%. Figure 8(f) is the influence of electrical stimulation intensity and pulse width of 1:0 CRS on the number of SWD. The increase of electrical stimulation intensity and pulse width will lead to the decrease of the SWD number, but the inhibition effect of increasing electrical stimulation intensity on SWD is more obvious than that of increasing electrical stimulation pulse width. Figure 8(g),(h) shows the effect of 3:2 CRS on neuronal activity. The change trend of the entire discharge activity was like the previous two, but the SWD area of 3:2 CRS accounts for 29.48%. Figure 8(i) shows the influence of stimulation intensity and pulse width of 3:2 CRS on the SWD number. Although the change trend of the SWD number is like the other electrical stimulation, the decrease trend of the SWD number is slow.

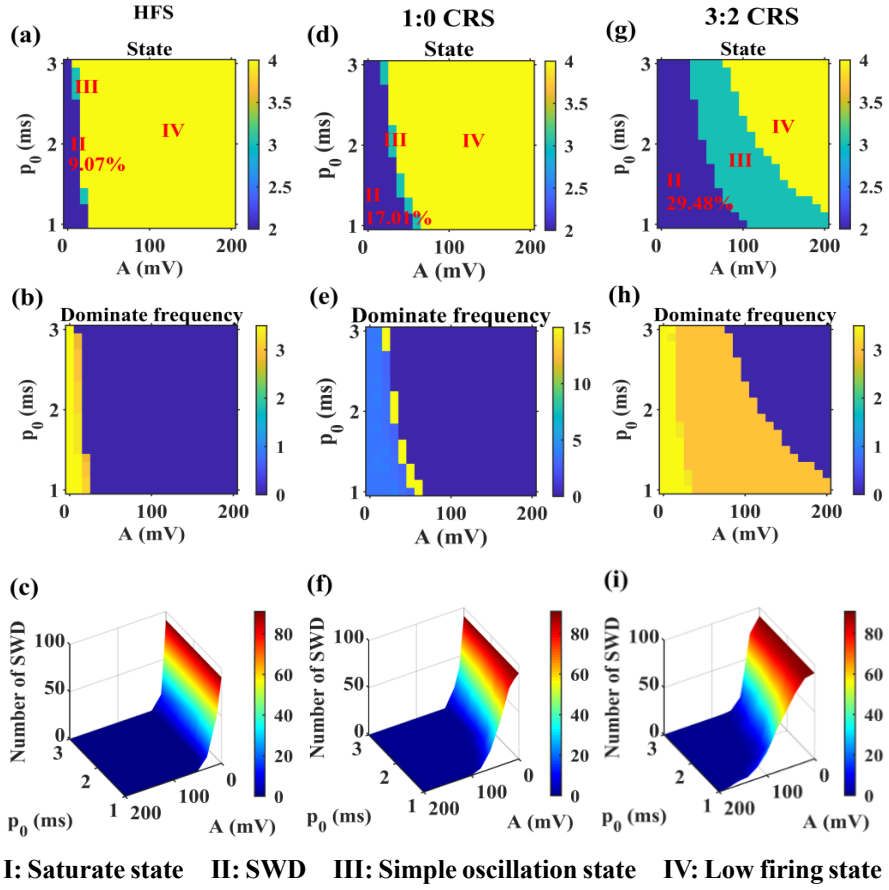

Figure 8. Influence of electrical stimulation on neuron dynamics in the (p_0, A) panel. (a) and (b) represent the influence of HFS on the dynamic states and oscillation frequency of neurons. (c) is the relationship between the stimulation intensity and frequency of HFS and the number of SWD. (d) and (e) represent the influence of 1:0 CRS on the dynamic state and oscillation frequency of neurons. (f) is the relationship between the stimulation intensity and frequency of 1:0 CRS and the number of SWD. (g) and (h) represent the influence of 3:2 CRS on the dynamic state and oscillation frequency of neurons. (i) is the relationship between the stimulation intensity and frequency of 3:2 CRS and the number of SWD. The period of electrical stimulation is $T = 120^{-1}$ s.

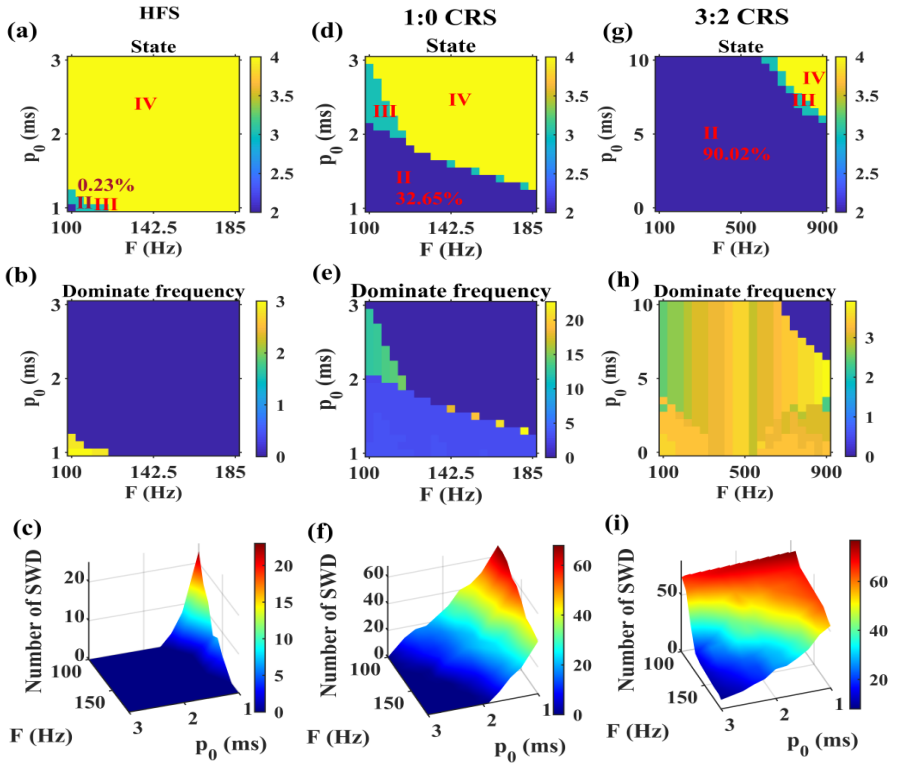

Figure 9. Influence of electrical stimulation on neuron dynamics in the (p_0, F) panel. (a) and (b) represent the influence of HFS on the dynamic state and oscillation frequency of neurons. (c) is the relationship between the stimulation intensity and frequency of HFS and the number of SWD. (d) and (e) represent the influence of 1:0 CRS on the dynamic state and oscillation frequency of neurons. (f) is the relationship between the stimulation intensity and frequency of 1:0 CRS and the number of SWD. (g) and (h) represent the influence of 3:2 CRS on the dynamic state and oscillation frequency of neurons. (i) is the relationship between the stimulation intensity and frequency of 3:2 CRS and the number of SWD. The intensity of electrical stimulation is $\mathrm{A} = 120$ mV.

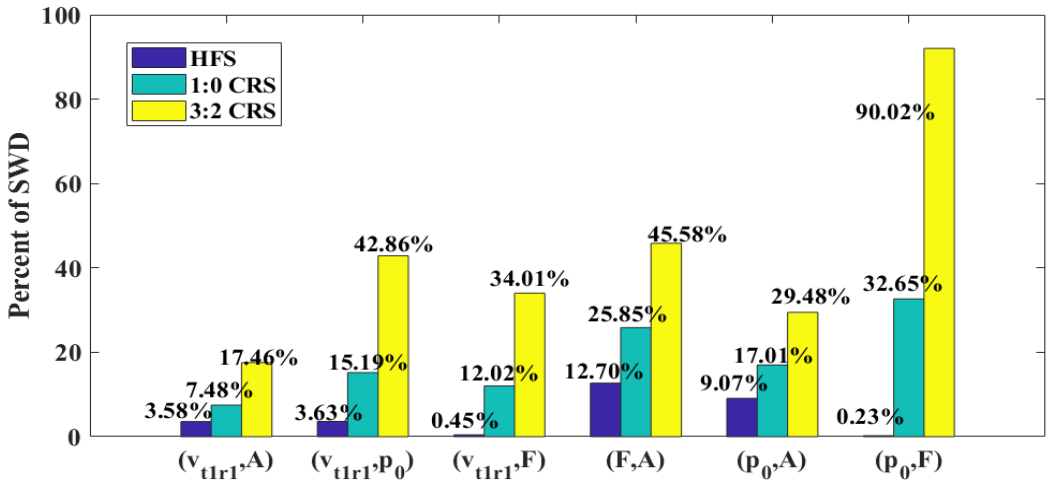

Figure 10. Effect of electrical stimulation on SWD percentage under different conditions.

Figure 9 shows the effect of electrical stimulation on neuronal dynamics in the (p_0, F) panel. Figure 9(a),(b) are the effects of HFS on the firing state and the frequency of neurons. Under the action of HFS, with the increase of electrical stimulation frequency and pulse width, the SWD area only accounts for 0.23% of the whole dynamic state. Figure 9(c) is the influence of pulse width and stimulation frequency of HFS on the number of SWD, from which we can know that with the increase of stimulation frequency and pulse width, the number of SWD will obviously decrease. Figure 9(d),(e) shows the impact of 1:0 CRS on neuron firing. The distribution of the SWD area was like Figure 9(a),(b), but the SWD area became larger, which accounts for 32.65%. The effect of 3:2 CRS on neuronal activity was shown in Figure 9(e),(f). Compared with HFS and 1:0 CRS, the SWD area of 3:2 CRS, the largest one accounts for 90.02%. Figure 9(i) is the influence of the pulse width and stimulation frequency of 3:2 CRS on the number of SWD, and its inhibition on the number of SWD is the worst among the three kinds of electrical stimulation. Figure 10 is a summary of the percentage of SWD under the above-mentioned different parameter combinations, from which we can know that HFS is obviously superior to CRS in inhibiting SWD. In addition, among the combination of coupling intensity and electrical stimulation parameters, the most obvious inhibitory effect of HFS on absence seizures is the combination of coupling intensity and electrical stimulation frequency, and the most obvious inhibitory effect of 1:0 CRS on absence seizures is the combination of coupling intensity and pulse width. The best inhibitory effect of 3:2 CRS on absence seizures is the combination of coupling intensity and electrical stimulation intensity. Among the combinations of electrical stimulation parameters, the combination of pulse width and electrical stimulation frequency showed that HFS had the best inhibitory effect on absence seizures. Under the combination of pulse width and electrical stimulation intensity, 1:0 CRS and 3:2 CRS had the most obvious inhibitory effect on absence seizures.

4. Conclusions

Based on the original BGCT model, we constructed a reduced BGCT-PPN model consisting of the PPN, two corticothalamic circuits and basal ganglia. We simplified the basal ganglia into a 3I:5O modulator for reducing the complexity of the model and iteration between neurons. We applied three forms of electrical stimulation to RE1 in the first corticothalamic circuit of the model, and then explored how the SWD region is inhibited by varying the parameters of electrical stimulation. By adjusting the parameters of electrical stimulation and the coupling strength of the model, we found that appropriately increasing the stimulation strength of electrical and the coupling strength of the model can effectively inhibit the SWD area. In addition, the increasing frequency and pulse width of electrical stimulation can also inhibit the SWD region.

The numerical results show that when the electrical stimulation pulse width is 1–3 ms, the electrical stimulation intensity is 0–200 mV, the stimulation frequency is 100–185 Hz and the SWD area will decrease with the increase of electrical stimulation parameters. Second, in different parameter panels, HFS has the most obvious inhibitory effect on SWD. 1:0 CRS also has a certain inhibitory effect on the SWD area, and the inhibitory effect is better than 3:2 CRS. These results are of great significance to the application of the mean field model in theoretical experiments and the exploration of how to regulate epilepsy through electrical stimulation parameters. It is hoped that our numerical simulation results will be helpful to clinical experiments. However, the above results are based on theoretical research and may have some limitations, so our next research plan is to test the results of theoretical research through experiments.

Use of AI tools declaration

The authors declare they have not used Artificial Intelligence (AI) tools in the creation of this article.

Data availability

The data used to support the findings of this study are included within the research.

Acknowledgments

This research was supported by the National Natural Science Foundation of China (Grant Nos. 12172210 and 11502139). The authors would like to thank the anonymous referees for their valuable comments.

Conflict of interest

The authors declare there is no conflict of interest.

References

1. Y. Chen, J. Lu, H. Pan, Y. Zhang, H. Wu, K. Xu, et al., Association between genetic variation of CACNA1h and childhood absence seizure, *Ann. Neurol.*, **54** (2003), 239–243. https://doi.org/10.1002/ana.10607
2. C. Wu, J. Xiang, W. Jiang, S. Huang, Y. Gao, L. Tang, et al., Altered effective connectivity network in childhood absence seizure: a multi-frequency MEG study, *Brain Topogr.*, **30** (2017), 673–684. https://doi.org/10.1007/s10548-017-0555-1
3. S. L. Moshe, E. Perucca, P. Ryvlin, T. R. Tomson, Epilepsy: New advances, *Lancet*, **385** (2015), 884–898. https://doi.org/10.1016/S0140-6736(14)60456-6
4. V. Crunelli, N. Leresche, Childhood absence seizure: Genes, channels, neurons and networks, *Nat. Rev. Neurosci.*, **3** (2002), 371–382. https://doi.org/10.1038/nrn811
5. B. S. Chang, D. H. Lowenstein, Epilepsy, *N. Engl. J. Med.*, **349** (2003), 1257–1266. https://doi.org/10.1056/NEJMra022308
6. A. Destexhe, Can $GABA_A$ conductances explain the fast oscillation frequency of absence seizures in rodents, *Eur. J. Neurosci.*, **11** (1999), 2175–2181. https://doi.org/10.1046/j.1460-9568.1999.00660.x
7. R. Guerrini, F. Melani, C. Brancati, A. R. Ferrari, P. Brovedani, A. Biggeri, et al., Dysgraphia as a mild expression of dystonia in children with absence seizure, *PLoS One*, **10** (2015), e0130883. https://doi.org/10.1371/journal.pone.0130883
8. H. Blumenfeld, K. J. Meador, Consciousness as a useful concept in seizure classification, *Epilepsia*, **55** (2014), 1145–1150. https://doi.org/10.1111/epi.12588
9. Z. Wang, Q. Wang, Stimulation strategies for absence seizures: Targeted therapy of the focus in coupled thalamocortical model, *Nonlinear Dyn.*, **96** (2019), 1649–1663. https://doi.org/10.1007/s11071-019-04876-z

10. E. Sitnikova, A. E. Hramov, V. Grubov, Time-frequency characteristics and dynamics of sleep spindles in WAG/Rij rats with absence seizure, *Brain Res.*, **1543** (2014), 290–299. https://doi.org/10.1016/j.brainres.2013.11.001
11. A. Kandel, G. Buzsáki, Cellular–synaptic generation of sleep spindles, spike-and-wave discharges, and evoked thalamocortical responses in the neocortex of the rat, *J. Neurosci.*, **17** (1997), 6783–6797. https://doi.org/10.1523/JNEUROSCI.17-17-06783.1997
12. R. L. Albin, A. B. Young, J. B. Penney, The functional anatomy of basal ganglia disorders, *Trends Neurosci.*, **18** (1995), 63–64. https://doi.org/10.1016/0166-2236(95)80020-3
13. A. Parent, L. N. Hazrati, Functional anatomy of the basal ganglia. I. The cortico-basal ganglia-thalamo-cortical loop, *Brain Res. Rev.*, **20** (1995), 91–127. https://doi.org/10.1016/0165-0173(94)00007-C
14. M. Chen, D. Guo, M. Li, T. Ma, S. Wu, J. Ma, et al., Critical roles of the direct GABAergic pallido-cortical pathway in controlling absence seizures, *PLoS Comput. Biol.*, **11** (2015), e1004539. https://doi.org/10.1371/journal.pcbi.1004539
15. D. Fan, Q. Wang, Closed-loop control of absence seizures inspired by feedback modulation of basal ganglia to the corticothalamic circuit, *IEEE Trans. Neural Syst. Rehabil. Eng.*, **28** (2020), 581–590. https://doi.org/10.1109/TNSRE.2020.2969426
16. P. A. Robinson, C. J. Rennie, D. L. Rowe, Dynamics of large-scale brain activity in normal arousal states and epileptic seizures, *Phys. Rev. E*, **65** (2002), 041924. https://doi.org/10.1103/PhysRevE.65.041924
17. M. Chen, D. Guo, T. Wang, W. Jing, Y. Xia, P. Xu, et al., Bidirectional control of absence seizures by the basal ganglia: A computational evidence, *PLoS Comput. Biol.*, **10** (2014), e1003495. https://doi.org/10.1371/journal.pcbi.1003495
18. P. Jiruska, M. De Curtis, J. G. Jefferys, C. A. Schevon, S. J. Schiff, K. Schindler, Synchronization and desynchronization in epilepsy: Controversies and hypotheses, *J. Physiol.*, **591** (2013), 787–797. https://doi.org/10.1113/jphysiol.2012.239590
19. H. F. J. Gonález, S. E. Goodale, M. L. Jacobs, K. F. Hass, B. A. Landman, V. L. Morgan, et al., Brainstem functional connectivity disturbances in epilepsy may recover after successful surgery, Neurosurgery, **86** (2020), 417. https://doi.org/10.1093/neuros/nyz128
20. T. Kita, H. Kita, Cholinergic and non-cholinergic mesopontine tegmental neurons projecting to the subthalamic nucleus in the rat: Pedunculopontine projection to subthalamus, *Eur. J. Neurosci.*, **33** (2011), 433–443. https://doi.org/10.1111/j.1460-9568.2010.07537.x
21. W. Thevathasan, B. Debu, T. Aziz, B. R. Bloem, C. Blahak, C. Butson, et al., Pedunculopontine nucleus deep brain stimulation in Parkinson's disease: A clinical review, *Mov. Disord.*, **33** (2018), 10–20. https://doi.org/10.1002/mds.27098
22. Y. Yu, H. Zhang, L. Zhang, Q. Wang, Dynamical role of pedunculopntine nucleus stimulation on controlling Parkinson's disease, *Physica A*, **525** (2019), 834–848. https://doi.org/10.1016/j.physa.2019.04.016
23. M. S. Lee, J. Q. Rinne, C. D. Marsden, The pedunculopontine nucleus: its role in the genesis of movement disorders, *Yonsei Med. J.*, **41** (2000), 167–184. https://doi.org/10.3349/ymj.2000.41.2.167
24. N. Jenkinson, D. Nandi, K. Muthusamy, N. J. Ray, R. Gregory, J. F. Stein, et al., Anatomy, physiology, and pathophysiology of the pedunculopontine nucleus, *Mov. Disord.*, **24** (2009), 319–328. https://doi.org/10.1002/mds.22189

25. P. A. Pahapill, A. M. Lozano, The pedunculopontine nucleus and Parkinson's disease, *Brain*, **123** (2000), 1767–1783. https://doi.org/10.1093/brain/123.9.1767
26. A. H. Niktarash, G. A. Shahidi, Effects of the activity of the internal globus palliduspedunculopontine loop on the transmission of the subthalamic nucleus-external globus pallidus-pacemaker oscillatory activities to the cortex, *J. Comput. Neurosci.*, **16** (2004), 113–127. https://doi.org/10.1023/B:JCNS.0000014105.87625.5f
27. H. L. Wang, M. Morales, Pedunculopontine and laterodorsal tegmental nuclei contain distinct populations of cholinergic, glutamatergic and GABAergic neurons in the rat, *Eur. J. Neurosci.*, **29** (2009), 340–358. https://doi.org/10.1111/j.1460-9568.2008.06576.x
28. P. Kwan, M. J. Brodie, Early identification of refractory epilepsy, *N. Engl. J. Med.*, **342** (2000), 314–319. https://doi.org/10.1056/NEJM200002033420503
29. J. Engel, S. Wiebe, J. Frence, M. Sperling, P. Williamson, D. Spencer, et al., Practice parameter: temporal lobe and localized neocortical resections for epilepsy: Report of the Quality Standards Subcommittee of the American Academy of Neurology, in association with the American Epilepsy Society and the American Association of Neurological Surgeons, *Neurology*, **60** (2003), 538–547. https://doi.org/10.1212/01.WNL.0000055086.35806.2D
30. K. Lehtimäki, J. W. Långsjö, J. Ollikainen, H. Heinonen, T. Möttönen, T. Tähtinen, et al., Successful management of super-refractory status epilepticus with thalamic deep brain stimulation, *Ann. Neurol.*, **81** (2017), 142–146. https://doi.org/10.1002/ana.24821
31. Z. Nanobashvili, T. Chachua, A. Nanobashvili, I. Bilanishvili, O. Lindvall, Z. Kokaia, Suppression of limbic motor seizures by electrical stimulation in thalamic reticular nucleus, *Exp. Neurol.*, **181** (2003), 224–230. https://doi.org/10.1016/S0014-4886(03)00045-1
32. Z. Wang, Q. Wang, Eliminating absence seizures through the deep brain stimulation to thalamus reticular nucleus, *Front. Comput. Neurosci.*, **11** (2017), 22. https://doi.org/10.3389/fncom.2017.00022
33. T. Wyckhuys, P. Boon, R. Raedt, B. Van Nieuwenhuyse, K. Vonck, W. Wadman, Suppression of hippocampal epileptic seizures in the kainate rat by Poisson distributed stimulation, *Epilepsia*, **51** (2010), 2297–2304. https://doi.org/10.1111/j.1528-1167.2010.02750.x
34. V. R. Cota, J. C. de Oliveira, L. C. M. Damázio, M. F. D. Moraes, Nonperiodic stimulation for the treatment of refractory epilepsy: Applications, mechanisms, and novel insights, *Epilepsy Behav.*, **121** (2021), 106609. https://doi.org/10.1016/j.yebeh.2019.106609
35. A. W. Quinkert, N. D. Schiff, D. W. Pfaff, Temporal patterning of pulses during deep brain stimulation affects central nervous system arousal, *Behav. Brain Res*., **214** (2010), 377–385. https://doi.org/10.1016/j.bbr.2010.06.009
36. M. Zeitler, P. A. Tass, Anti-kindling induced by two-stage coordinated reset stimulation with weak onset intensity, *Front. Comput. Neurosci.*, **10** (2016), 44. https://doi.org/10.3389/fncom.2016.00044
37. M. Zeitler, P. A. Tass, Augmented brain function by coordinated reset stimulation with slowly varying sequences, *Front. Syst. Neurosci.*, **9** (2015), 49. https://doi.org/10.3389/fnsys.2015.00049
38. D. Fan, Q. Wang, Improving desynchronization of parkinsonian neuronal network via tripletstructure coordinated reset stimulation, *J. Theor. Biol.*, **370** (2015), 157–170. https://doi.org/10.1016/j.jtbi.2015.01.040
39. C. R. Pantoja-Jiménez, V. M. Magdaleno-Madrigal, S. Almazán-Alvarado, R. Fernández-Mas, Anti-epileptogenic effect of high-frequency stimulation in the thalamic reticular nucleus on PTZ-induced seizures, *Brain Stimul.*, **7** (2014), 587–594. https://doi.org/10.1016/j.brs.2014.03.012

40. C. J. Rennie, P. A. Robinson, J. J. Wright, Effects of local feedback on dispersion of electrical waves in the cerebral cortex, *Phys. Rev. E*, **59** (1999), 3320–3329. https://doi.org/10.1103/PhysRevE.59.3320
41. P. A. Robinson, C. J. Rennie, D. L. Rowe, S. C. O'Connor, A. E. Gordon, Multiscale brain modelling, *Phil. Trans. R. Soc. B*, **360** (2005), 1043–1050. https://doi.org/10.1098/rstb.2005.1638
42. S. J. van Albada, P. A. Robinson, Mean-field modeling of the basal ganglia-thalamocortical circuit. I: Firing rates in healthy and parkinsonian states, *J. Theor. Biol.*, **257** (2009), 642–663. https://doi.org/10.1016/j.jtbi.2008.12.018
43. M. Breakspear, J. A. Roberts, J. R. Terry, S. Rodrigues, N. Mahant, P. A. Robinson, A unifying explanation of primary generalized seizures through nonlinear brain modeling and bifurcation analysis, *Cereb. Cortex*, **16** (2006), 1296–1313. https://doi.org/10.1093/cercor/bhj072
44. F. Marten, S. Rodrigues, O. Benjamin, M. P. Richardson, J. R. Terry, Onset of polyspike complexes in a mean-field model of human electroencephalography and its application to absence seizure, *Phil. Trans. R. Soc. A.*, **367** (2009), 1145–1161. https://doi.org/10.1098/rsta.2008.0255
45. F. Freyer, J. A. Roberts, R. Becker, P. A. Robinson, P. Ritter, M. Breakspear, Biophysical mechanisms of multistability in resting-state cortical rhythms, *J. Neurosci.*, **31** (2011), 6353–6361. https://doi.org/10.1523/JNEUROSCI.6693-10.2011
46. S. J. van Albada, R. T. Gray, P. M. Drysdale, P. A. Robinson, Mean-field modeling of the basal ganglia-thalamocortical circuit. II: Dynamics of parkinsonian oscillations, *J. Theor. Biol.*, **257** (2009), 664–688. https://doi.org/10.1016/j.jtbi.2008.12.013
47. B. Hu, D. Guo, Q. Wang, Control of absence seizures induced by the pathways connected to SRN in corticothalamic circuit, *Cognit. Neurodyn.*, **9** (2015), 279–289. https://doi.org/10.1007/s11571-014-9321-1
48. P. A. Robinson, C. J. Rennie, D. L. Rowe, Dynamics of large-scale brain activity in normal arousal states and epileptic seizures, *Phys. Rev. E*, **65** (2002), 041924. https://doi.org/10.1103/PhysRevE.65.041924
49. S. M. Alavi, A. Mirzaei, A. Valizadeh, R. Ebrahimpour, Excitatory deep brain stimulation quenches beta oscillation arising in a computational model of the subthalamo-pallidal loop, *Sci. Rep.*, **12** (2022), 7845. https://doi.org/10.1038/s41598-022-10084-4
50. C. Liu, Y. Yao, J. Wang, H. Li, H. Hu, K. A. Loparo, et al., Oscillation suppression effects of intemittent noisy deep brain stimulation induced by coordinated reset pattern based on a computational model, *Biomed. Signal Process. Control*, **73** (2022), 103466. https://doi.org/10.1016/j.bspc.2021.103466
51. A. Destexhe, Spike-and-wave oscillations based on the properties of $GABA_B$ receptors, *J. Neurosci.*, **18** (1998), 9099–9111. https://doi.org/10.1523/JNEUROSCI.18-21-09099.1998
52. R. L. Macdonald, J. Q. Kang, M. J. Gallagher, H. J. Feng, $GABA_A$ receptor mutations seizure associated with generalized epilepsies, *Adv. Pharmacol.*, **54** (2006), 147–169. https://doi.org/10.1016/S1054-3589(06)54007-4
53. J. L. Noebels, M. Avoli, M. Rogawski, R. Olsen, A. V. Delgado-Escueta, "Jasper's basic mechanisms of the epilepsies" workshop, *Epilepsia*, **51** (2010), 1–5. https://doi.org/10.1111/j.1528-1167.2010.02792.x